Journal of Theoretical Biology 347 (2014) 54–62

Contents lists available at ScienceDirect

Journal of Theoretical Biology

journal homepage: www.elsevier.com/locate/yjtbi

A dynamic dosimetry model for radioactive exposure scenarios in *Arabidopsis thaliana*

Geert Biermans [a,b,*], Nele Horemans [a], Niel Hens [c,d], Jordi Vives i Batlle [a], Hildegarde Vandenhove [a], Ann Cuypers [b]

[a] SCK•CEN, Biosphere Impact Studies, Boeretang 200, 2400 Mol, Belgium
[b] Centre for Environmental Research, Hasselt University, Agoralaan 1, 3590 Diepenbeek, Belgium
[c] Center for Statistics, Hasselt University, Agoralaan 1, 3590 Diepenbeek, Belgium
[d] Centre for Health Economic Research and Modelling Infectious Diseases, Vaccine and Infectious Disease Institute, University of Antwerp, Universiteitsplein 1, 2610 Antwerp, Belgium

HIGHLIGHTS

- A dynamic dosimetry model is proposed for *Arabidopsis thaliana* including growth and uptake.
- The influence of growth on dosimetry depends on the radionuclide involved.
- Use of dynamic dosimetry models improves the dose calculations for effect studies.

ARTICLE INFO

Article history:
Received 21 May 2013
Received in revised form
7 January 2014
Accepted 7 January 2014
Available online 16 January 2014

Keywords:
Plant dosimetry
Arabidopsis thaliana
Radiological protection
Exposure modelling

ABSTRACT

To obtain a better understanding on how non-human biota are affected by exposure to environmental radioactivity, it is essential to link observed effects to a correct estimate of absorbed ionising radiation dose. Current wildlife dose rate and risk assessment tools are not set up to assess changes in dose rate during organism development. This paper presents a dosimetry model for assessing dose rate and absorbed dose during seedling development of the model plant *Arabidopsis thaliana*. We included growth and radionuclide absorption dynamics into the dose calculations. This model was subsequently used to compare the dose and dose rate calculations for three radionuclides, ^{241}Am (α-radiation), ^{90}Sr (β-radiation) and ^{133}Ba (γ-radiation), in a standard exposure scenario. We show that growth influences dose and dose rate and that this influence depends on the radionuclide and the organ involved. The use of dynamic dosimetry models greatly improves the dose calculations for effect studies.

1. Introduction

Anthropogenic levels of radioactivity in the environment are ever increasing, either as routine releases by nuclear power plants and the NORM industries, or by accidental releases such as that of the recent Fukushima accident. Evaluating the risks associated with the presence of radioactive material in the environment not only necessitates a description of the interaction and transport of radionuclides with and within the biosphere, but also requires a good understanding of the delivered dose and the adverse effects it may cause in biota. International effort has therefore been made, both by regulatory bodies and by the scientific community, to build a radiological environmental protection system. Environmental protection benchmarks have been derived by different organisations (Garnier-Laplace and Gilbin 2006; Andersson et al., 2009; ICRP, 2009), and protection may be rather at the ecosystem level (Garnier-Laplace and Gilbin, 2006) or rather at the organism group level or individual level (ICRP, 2009). Comparison of the dose rate assessment results with the benchmark values allows to make a judgement in how far the contamination or exposure to radioactivity affects the wildlife or is of no environmental concern. Gaps in our present understanding of radionuclide transfer to biota and low-dose radiation effects and the subsequent extrapolations and uncertainty in the dosimetric calculations over an organism life span, contributes to a considerable amount of uncertainty in risk assessment for non-human biota (Garnier-Laplace et al., 2004).

Hitherto, the dosimetric approach used within environmental risk assessment software tools such as ERICA (Brown et al., 2008)

* Corresponding author at: SCK•CEN, Biosphere Impact Studies, Boeretang 200, 2400 Mol, Belgium. Tel.: +321 433 2115.
E-mail address: geert.biermans@gmail.com (G. Biermans).

0022-5193/$ - see front matter © 2014 Elsevier Ltd. All rights reserved.
http://dx.doi.org/10.1016/j.jtbi.2014.01.012

has been based upon absorbed energy fractions of radioactive decay within a given geometry. In all models commonly used for calculating dose to non-human biota (including the present one), the reference organism is reduced to a single ellipsoid, which is defined by its three axes. A stochastic method is used to calculate the fraction of energy absorbed within the body as a function of decay energy. This approach allows for the calculation of a dose conversion coefficient (*DCC*, $\mu Gy\ h^{-1}/Bq\ kg^{-1}$ or $Bq\ L^{-1}$) for each radionuclide whose decay pathways and quantum yield are known (Copplestone et al., 2001). This *DCC* value reflects how much of the decay energy is absorbed inside the organism per unit contamination in the environmental media (external exposure) or in the body (internal exposure). It is specific to the defined geometry of organism and exposure medium (and homogeneous/inhomogeneous distribution of the radioactivity in media and body) and converts a known or calculated radionuclide activity concentration into a dose rate, which can then be used to integrate the absorbed dose over exposure time. When we want to understand the effects of radiation exposure, we need a robust estimation of the dose rate and absorbed doses delivered to the exposed organisms (Copplestone et al., 2001; Hinton et al., 2013). In a foregoing study, we described a simple dose rate assessment approach for the model plant *Arabidopsis thaliana* based on the geometries for root and shoot organs and radionuclide incorporation at the end of the hydroponic growth experiment. We compared the exposure for three types of radiation (α, β and γ) (Biermans et al., 2013). Our study showed that dose assessment can be improved by providing a more detailed description of the biota geometry, i.e. by describing each organ separately (i.e. root and shoot) and by considering the radionuclide distributions between the organs. We also showed that internal *DCC* values for some of the radionuclides were quite sensitive to changes in geometry. This means that the rapid changes in shoot and root size during growth of *A. thaliana* seedlings are likely to affect the dose during radionuclide exposure. By including growth dynamics in the dosimetric calculations, we can therefore obtain an improved estimation of dose rates and doses delivered during the time of exposure.

Our aim in this study is to develop an improved dosimetric model for *A. thaliana* seedlings under hydroponic growth, based upon the dosimetric principles described above, and further taking into account the rapid changes in geometry of the organs during early growth and changes in radionuclide uptake. We then use this model to calculate the dose rates and absorbed doses delivered to roots and shoots in an exposure scenario of different radiation quality (α, β, and γ radiation). Finally, we compared our dose predictions with those obtained for a non-dynamic dose assessment.

2. Methods

2.1. Experimental setup

To introduce growth dynamics into the dosimetry model, we needed to measure the changes in geometry during growth for the roots and shoots of *A. thaliana* seedlings, and calculate the resulting theoretical changes in *DCC* for ^{241}Am, ^{90}Sr and ^{133}Ba. This allows for comparison with the data from our previous study (Biermans et al., 2013), which uses these radionuclides in an exposure setup. We selected the time interval between 96 and 504 h or 21 days after seeding, as this is a period of rapid plant growth and the preferred growth period for exposure experiments on *Arabidopsis* seedlings.

2.2. Plant culture

Prior to sowing, *A. thaliana* (Columbia ecotype) were spread-out on moist filter paper and vernalized for three days at 4 °C to synchronize germination. The seeds were subsequently sown on plugs from 1.5 mL eppendorf tubes filled with 0.6% agar in modified Hoagland solution (1 mM KNO_3, 0.3 mM $Ca(NO_3)_2$, 0.2 mM $MgSO_4$, 0.1 mM $NH_4H_2PO_4$, 1.62 μM $FeSO_4$, 0.78 μM Na_2EDTA, 4.6 μM H_3BO_3, 0.9 μM $MnCl_2$, 0.032 μM $CuSO_4$, 0.055 μM H_2MoO_4, 0.077 μM $ZnSO_4 \cdot 7H_2O$). The plugs were mounted on a PVC cover, capable of holding 36 plugs, after which each cover was placed on a container filled with 1.35 L modified Hoagland solution.

Plants were grown in a growth chamber (Microclima 1000E, Snijders Scientific B.V.) under a 16/8 day/night photoperiod with 22 °C/16 °C day/night temperatures and 65% relative humidity. Photosynthetic photon flux density was 100 $\mu mol\ m^{-2}\ s^{-1}$ at the leaf level (Sylvania BriteGro F36WT8/2084 and F36WT8/2023 lamps). The nutrient medium was aerated with a peristaltic pump from 7 days after sowing onwards and was replaced every 3 days.

2.3. Biometry

Plant growth was monitored between 4 and 21 days after sowing. The rosette area was measured with ImageJ software on pictures taken at several time points within the growth interval (Leister et al., 1999; Schneider et al., 2012). Root length was determined after 7, 10 and 21 days by measuring maximum length of the main root on a ruler as in Biermans et al. (2013).

2.4. DCC calculations

To determine the *DCC* for each plant age, we used an improved version of the Monte Carlo method described in detail by Copplestone et al. (2001), Vives I Batlle et al. (2004), which calculates the *DCC* value for a given ellipsoid geometry and a given radionuclide. This method is based on an iterative calculation of the probability of absorption of a radioactive particle across a large number of possible trajectories within the geometry, defined randomly.

2.4.1. Defining ellipsoid geometries

The leaf geometries for each time point were derived from the rosette area values measured in Section 2.3. This total leaf area was then defined as a circle with diameter *D*, which forms the cross-section through the centre of the ellipsoid. The third dimension, defining the leaf thickness, was kept identical for all time points at 0.15 cm as a simplifying assumption to facilitate calculations. We describe the ellipsoid geometry here for convenience as $2a_1 \times 2a_2 \times 2a_3$, with a_1, a_2 and a_3 the three semi-axes of the ellipsoid. For a given diameter *D*, the geometry was therefore defined as $D \times D \times 0.15$ cm with density 1. Root ellipsoid geometries for each time point were defined as using a constant root diameter of 100 μm. The third axis was defined as the root length determined under Section 2.3.

2.4.2. Calculation of absorbed energy fractions

These geometries were then used as input for the Monte Carlo calculation method for absorbed fractions as a function of decay energy. This method uses point-specific absorbed fractions (AF) for γ rays (Berger, 1968). For β particles, Berger's tabulated values of r_p (the radius *r* of a sphere within which *p*% of the energy is absorbed from a point β source located at the centre) were used (Berger, 1971). These values were transformed to values of fractional absorption from a point β emitter within a sphere of radius equal to r/r_{90} around the source, which makes the fractional absorption relatively independent of energy. For α-particles, the absorbed fraction was defined as being 1 for all geometries used, due to the short range of the particles in living tissue. Absorbed fractions as a function of decay energy E_d for γ- and β-particles were respectively

fitted to the functions (1) and (2) (Vives I Batlle et al., 2004):

$$F\gamma(E_d) = \exp\left(-\left(\frac{E}{2\sigma}\right)^n\right) + a \times exp(-\lambda E^m) \quad (1)$$

$$F_\beta(E_d) = \frac{1}{1+bE^q} \quad (2)$$

with σ, n, a, λ and m as fitted parameters for $F_\gamma(E_d)$ and b and q for $F_\beta(E_d)$.

We adapted the original Excel VBA code used for the absorbed fraction calculation into the programming language for the statistical software R (R Development Core Team, 2011). This enabled us to perform the calcuations much faster and automate them for a large series of geometries operating in a batch mode. Absorbed fractions for each geometry at 18 energy values (0.015–3 MeV) were calculated with 50,000 iterations, sufficient for the values to converge enough to keep the uncertainty at $\leq 2\%$ (2σ) for the β-values and $\leq 10\%$ (2σ) for the γ-values.

To fit the AF values to Eqs. (1) and (2), the original VBA tool relied on manual estimation of the starting parameters σ, n, a, λ and m or b and q. Then, the Excel solver add-on was used to minimize the sum of squared deviations (χ^2). While we used this method for $F_\beta(E_d)$, estimation of the parameters for $F_\gamma(E_d)$ proved more difficult due to the convergence to local minima, especially for small geometries. To fit $F_\gamma(E_d)$ we therefore used a combination of an elitist genetic algorithm (GA) based upon Gulsen et al. (1995) and the Levenberg–Marquardt fit algorithm (Marquardt, 1963) included in the *minpack.lm* package for R (Elzhov et al., 2010).

The GA for $F_\gamma(E_d)$ was run on a large initial population with size N of parameter combinations, with each parameter randomly drawn from a uniform distribution devoid of lower or upper boundaries. During every iteration, the data were first fitted to the $F_\gamma(E_d)$ function formed by each parameter set, recording χ^2 as a value for fitness. About 50% of the individuals with the highest fitness (i.e. the lowest value for χ^2) were then retained and defined as the *parent population*, of which one half was subsequently crossed-over with the second half in random pairs, forming 'offspring' with randomly shuffled values for each parameter compared with their parent pair. This was defined as the *crossover population*. A second offspring population was created by randomly sampling half of the parent population and multiplying the parameter values by the range of the parameter values in this subpopulation and a mutation factor. This mutation factor was drawn randomly for each parameter during each iteration from a uniform distribution with lower and upper limits ($-K$, K). The resulting *mutated population* was then reunited with the *parent population* and the *crossover population* into a single population which was then used in the next iteration.

We ran the algorithm with $N=10{,}000$, $K=5$ and 15 iterations, whereupon the values from the parameter set with the highest fitness value were used as the starting parameters in the Levenberg–Marquardt algorithm. This combination of GA and Levenberg–Marquardt was run a 100 times, after which the parameter set with the best fit was selected for *DCC* calculation. Previous tests of this combined algorithm showed that this gives a 99% probability to obtain stable resultant parameter values.

2.4.3. Calulation of DCC values

The resulting parameter sets for $F_\beta(E_d)$ and $F_\gamma(E_d)$ for each geometry were used to calculate the internal *DCC* values (unweighted by radiation quality) for ^{241}Am, ^{90}Sr and ^{133}Ba. *DCC*'s (in μGy h^{-1}/Bq kg^{-1}) for each radionuclide are obtained by summation of the decay pathways of the radionuclide in question and those of its chain of daughter radionuclides, each multiplied by (a) the associated AF at that energy (as derived from Eqs. (1) and (2)) and (b) a conversion factor of 5.77×10^{-4} between MeV s^{-1} and μJ h^{-1}. Where relevant, the tool included daughters in equilibrium with parent radionuclides, as judged to occur in the environment. External *DCC* values are obtained in the same way, but by substituting AF by $(1-\text{AF})$ in the calculations. The method is given in detail in Vives I Batlle et al. (2004).

3. Exposure model

The aim of our model is to be able to predict dose rates and total absorbed doses during development of *A. thaliana* seedlings exposed to different types of radiation by uptake of radionuclides from a liquid medium.

3.1. General model

The *DCC* value converts activity concentration (*AC*), the measure of radioactivity in the tissue or surrounding water (in Bq kg^{-1} or Bq L^{-1}), into a dose rate, which describes the amount of energy deposed into the living tissue per kg per unit of time (here in μGy h^{-1}). Therefore, at any given moment in the exposure, the dose rate can be calculated by multiplying the *AC* and *DCC* at that time point. Though calculation of the *DCC* value is only dependent on geometry in our method, values for *AC* can be obtained in several ways. An important point here is that the biota respond dynamically to the medium activity concentration. This will be further discussed in more detail below.

3.1.1. External exposure

The external dose rate is delivered by the surrounding medium, which activity concentration is measured during the course of an experiment and for which sampling is usually not limited. For an experiment where the external media concentration remains constant during the exposure, the external dose rate can be described as in Eq. (3) and is time-independent.

$$DR_{ext}(t) = AC_{ext} \times DCC_{ext}(t) \quad (3)$$

with AC_{ext} the activity concentration in the hydroponic medium, DCC_{ext} the external *DCC* value at time t and DR_{ext} the resulting external dose rate at that time point. The total dose delivered between the start of the exposure, S and for the duration of the exposure, E, equals the integral of Eq. (4) between time points S and $S+E$.

$$Dose_{ext}(S,\ E) = AC_{ext} \times \int_S^{S+E} DCC_{ext}(t)dt \quad (4)$$

3.1.2. Internal exposure

Internal dose rate depends on the internal activity concentration of the radionuclide in the tissue or organ and the homogeneity by which activity is distributed within the organism. This can either be calculated based on values for medium-to-tissue concentration ratios available in literature for a number of radionuclides (IAEA, 2010), or measured directly by analysing the tissue.

Both methods have their specific advantages and disadvantages. While concentration ratios do not require measurement of internal biota concentrations, they are prone to high variability and are dependent on environmental conditions and species resulting in a 'compound parameter' that can span several orders of magnitude. For elements and species for which no transfer parameters are available, the values are interpolated based upon rules such as chemical or species similarity (Beresford et al., 2009). This makes it preferable to work with measured activity concentrations where possible, even if it relies on destructive measurements, which use material that might otherwise be available for analysis of biological endpoints. Radioecological risk assessment

tools such as ERICA can handle both types of input, but use measured activity concentrations when available.

We therefore chose to base our dose (rate) assessment model on the concept of an experimentally determined *AC* at the end of the exposure period. Risk assessment tools such as ERICA and RESRAD-BIOTA (DOE, 2011) assume instantaneous equilibrium between environment and living tissue, which means that the *AC* measured at the end of the experiment is assumed to be constant from the start of the exposure. This is unlikely a valid assumption since biological and environmental processes are dynamic (Vives I Batlle, 2011; Psaltaki et al., 2013) and for more accurate dose assessment a growth stage dependent uptake was considered.

Based on earlier experiments (Biermans et al., 2013), we showed that that the accumulation of the radionuclides considered inside a plant organ is linear in time for exposure lengths up to 7 days (168 h). We here assume that the accumulation rate (α, Bq kg^{-1} h^{-1}) remains constant for seedlings exposed between 96 h and 504 h after seeding. Under this assumption, the radionuclide-specific accumulation rate for a given tissue can be calculated by dividing the *AC* of the radionuclide of interest measured at the end of exposure, by the exposure duration of the experiment.

$$\alpha = \frac{AC_{end}}{E_{experiment}} \tag{5}$$

The change of *AC* with exposure time can then be described by Eq. (6), which calculates the radionuclide accumulation from the start of the exposure.

$$AC(t) = \alpha(t-S) \text{ so that } AC \geq 0 \text{ for } t \geq S \tag{6}$$

The internal dose rate at time $S+E$ can then be described by adapting Eq. (3) into an equation with *AC* dependent on time (Eq. (7))

$$DR_{int}(t) = \alpha(t-S) \times DCC_{int}(t)$$
$$DR_{int}(S,E) = \alpha E \times DCC_{int}(S+E) \tag{7}$$

Similarly, total internal dose then becomes

$$Dose_{int}(S,\ E) = \int_{S}^{S+E} \alpha(t-S) \times DCC_{int}(t)dt \tag{8}$$

Combining each of Eqs. (3), (4), (7) and (8) with the obtained data for *DCC(t)*, we can make the dosimetric model for each plant organ account for growth.

3.2. Shoot dosimetry

In aquatic hydroponic exposure experiments, the shoot is only exposed internally to radionuclides transported to the shoot tissue from the roots. The external dose can be neglected. The internal *DCC* values for the different growth stages of *A. thaliana* seedlings were obtained by defining the geometry for each stage, based on the rosette area (Section 2.4). Table 1 lists the measured area values and the derived diameter *D* for the Monte Carlo calculations.

To define the internal $DCC_{shoot}(t)$ for each radionuclide, we fitted the values to a logarithmic function of the form $b+c\ ln(t)$. This function most accurately described *DCC* as a function of time for all three radionuclides and for the time interval studied. Fig. 1A–C shows the calculated *DCC* values and the fitted *DCC(t)* curve for each radionuclide. Table 2 lists the fitted values for parameters *b* and *c* for each fit, the adjusted r^2 and sigma, i.e. the standard deviation of the random error. The results show that the function is able to accurately predict the *DCC* for all three elements for t=[96,504].

Table 1
Rosette area and derived *D* values for each time point (in hours after seeding; HAS) used in the Monte Carlo *DCC* calculations on ellipsoid geometry (0.15 cm × *D* × *D*). Standard error on rosette area is < 2% for all time points with $N > 30$.

Time (HAS)	Rosette area (cm²)	*D* (cm)
96	0.01	0.11
120	0.02	0.16
168	0.04	0.23
240	0.08	0.32
264	0.13	0.41
288	0.19	0.49
312	0.25	0.57
336	0.34	0.66
408	0.83	1.03
432	1.07	1.17
456	1.41	1.34
480	1.78	1.51
504	2.18	1.67

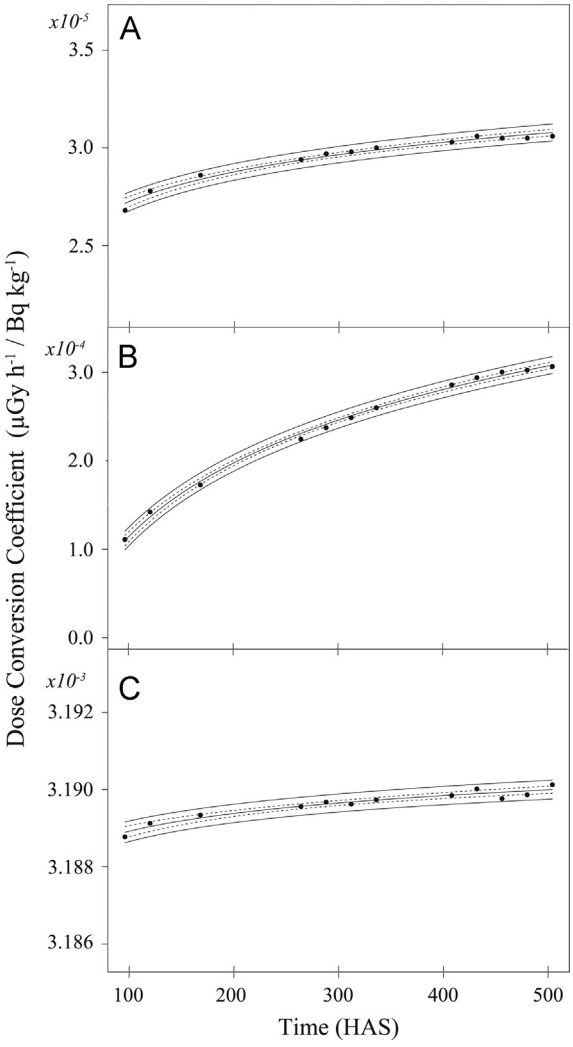

Fig. 1. Internal Shoot Dose conversion coefficients (*DCC*). Values are presented as a function of time (in hours after sowing) for ^{133}Ba (A), ^{90}Sr (B) and ^{241}Am (C). Confidence (dashed line) and prediction bands (solid line) for the fitted model $DCC(t)=b+c\ ln(t)$ are shown.

By introducing $DCC_{shoot}(t)$ into Eq. (7), the internal shoot dose rate after exposure length *E* (at $t=S+E$) equals

$$DR_{shoot,\ int}(S,E) = \alpha E \times (b + c\ \ln(S+E)) \tag{9}$$

Table 2
Fitted $DCC(t)$ parameters for internal shoot dosimetry for ^{133}Ba ^{90}Sr and ^{241}Am. The function $DCC(t)=b+c\ln(t)$ was fitted to the calculated DCC values for each radionuclide. For each radionuclide both parameters and their 95% confidence interval (CI) are given as well as the adjusted r^2 value for goodness-of-fit and the standard deviation of random error sigma.

			b	95% CI	*c*	95% CI	Adjusted r^2	Sigma
γ	**^{133}Ba**	Fig. 1A	1.720×10^{-5}	$[1.595-1.845]\times10^{-5}$	2.184×10^{-6}	$[1.964-2.404]\times10^{-6}$	0.978	1.811×10^{-7}
β	**^{90}Sr**	Fig. 1B	-4.360×10^{-4}	$[-4.633--4.087]\times10^{-4}$	1.196×10^{-4}	$[1.148-1.244]\times10^{-4}$	0.996	3.964×10^{-6}
α	**^{241}Am**	Fig. 1C	3.186×10^{-3}	$[3.185-3.187]\times10^{-3}$	6.673×10^{-7}	$[5.447-7.899]\times10^{-7}$	0.930	1.011×10^{-7}

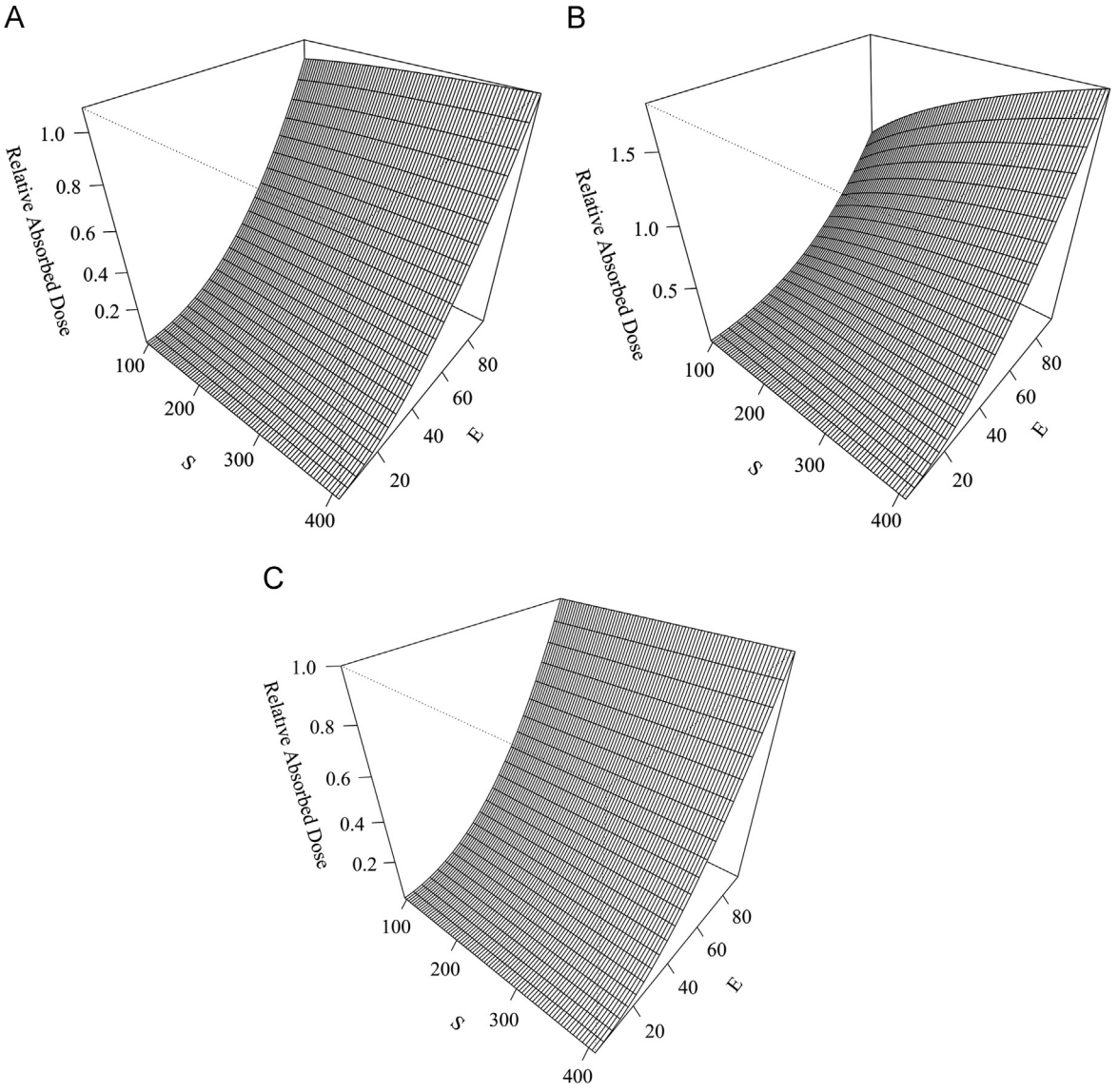

Fig. 2. Shoot dosimetry models for ^{133}Ba (A), ^{90}Sr (B) and ^{241}Am (C). Calculations are shown for start of exposure S (in hours after sowing) between 96 and 408 h after seeding with exposure length E (in hours) from 0 to 96 h. Doses are expressed as a ratio to the dose at $S=96$ h, $E=96$ h.

Similarly, total dose for a given starting point S and exposure length E, by expansion of Eq. (8) and by solving the integral, becomes

$$Dose_{shoot,int}(S,E)=\alpha\int_{S}^{S+E}(t-S)\times(b+c\ln(t))dt$$
$$=\frac{\alpha}{2}\left[bE^2+c\left((S^2(\ln(S)-\ln(S+E)))+\left(\frac{E^2(2\ln(S+E)-1)}{2}\right)+ES\right)\right] \quad (10)$$

Transects for a specific value of S give the evolution of accumulated dose during exposure. Conversely, transects for a given exposure length E represent the dose at the end of the exposure as a function of the starting point during the seedlings' growth.

Fig. 2A–C shows the absorbed dose for each radionuclide for an exposure with S from 96 h to 408 h after seeding (HAS) and a maximum exposure length of 96 h. The absorbed dose is expressed relative to the dose value for $S=96$ h and $E=96$ h. As α is constant and therefore outside of the integral in Eq. (10), the relative difference between two points on the surface is independent of α.

A relative 95% confidence interval (CI) was constructed for each point of the surface using the parametric bootstrap method

Table 3
Root length and calculated external and internal root *DCC* values for ^{133}Ba ^{90}Sr and ^{241}Am. Ellipsoid geometry for *DCC* calculation at each time point (in hours after seeding; HAS) was (0.01 cm × 0.01 cm × root length). Standard error on root length is < 3% with $N > 20$.

Time (HAS)	Root length (cm)	External *DCC* [μGy h^{-1}/Bq L^{-1}]			Internal *DCC* [μGy h^{-1}/Bq L^{-1}]		
		^{133}Ba	^{90}Sr	^{241}Am	^{133}Ba	^{90}Sr	^{241}Am
96	2.1	2.429E−04	6.315E−04	2.313E−05	1.953E−05	2.081E−05	3.185E−03
168	3.3	2.430E−04	6.315E−04	2.314E−05	1.950E−05	2.078E−05	3.185E−03
240	4.8	2.429E−04	6.315E−04	2.313E−05	1.953E−05	2.076E−05	3.185E−03
504	10.2	2.429E−04	6.315E−04	2.313E−05	1.953E−05	2.076E−05	3.185E−03

(Davison and Hinkley, 1997), drawing random newly predicted *DCC* values from a normal distribution with standard deviation σ (Table 2). The number of bootstraps equalled 5000 for each data point. The average relative 95% CI was 2.00% for ^{133}Ba, 5.9% for ^{90}Sr and 0.01% for ^{241}Am.

3.3. Root dosimetry

Roots receive external exposure from the radionuclides in the surrounding hydroponic medium as well as internally from the radionuclides absorbed into the tissue. Root lengths and the derived external and internal *DCC*'s are shown in Table 3. These data show that external and internal root *DCC* did not increase or decrease more than 1% for either of the radionuclides studied between the first measurement at 96 h and the last time point at 504 h after seeding. This is in contrast with the shoots, where changes in geometry during growth has much larger influence on *DCC*, except for ^{241}Am. For the roots, we can therefore assume that *DCC(t)* is a constant within the interval $t=[96,504]$ for the three radionuclides. The external dose rate (Eq. (11)) and internal dose (Eq. (12)), derived from Eqs. (3) and (4), can then be derived for the root-specific form

$$DR_{root,ext}(S,E) = AC_{ext} \times DCC_{root,ext} \tag{11}$$

$$Dose_{root,ext}(S,\ E) = AC_{ext} \times DCC_{root,ext} \int_{S}^{S+E} dt$$
$$= AC_{ext} \times DCC_{root,ext} \times E \tag{12}$$

We can conclude from the foregoing that the dose rate delivered to the roots by the medium is constant, and that the total absorbed dose after exposure length E is independent of the exposure starting point.

The internal root dose rate (Eq. (13)) and dose (Eq. (14)) can be derived from Eqs. (7) and (8) in a similar way. Again, both equations are independent of the timing of the exposure.

$$DR_{root,int}(S,E) = DCC_{root,int} \times \alpha E \tag{13}$$

$$Dose_{root,int}(S,\ E) = \alpha \times DCC_{root,int} \times \int_{S}^{S+E} (t-S)dt$$
$$= DCC_{root,int} \times \frac{\alpha E^2}{2} \tag{14}$$

4. Results and discussion

The main aim of this study was to develop a plant dosimetry model that integrates growth and variations in radionuclide uptake into the calculations. The backbone of the model is the calculation of the *DCC* values for the three representative radionuclides, ^{241}Am (α), ^{90}Sr (β) and ^{133}Ba (γ), as a function of time (seedling development).

It is clear from the internal *DCC* values for the leaves (Fig. 1A–C) that shoot growth influences the evolution of the *DCC* values over time, but not to the same extent for every radiation type. Whereas the *DCC* for β-emitter ^{90}Sr increased nearly 3-fold between 96 h and 504 h after seeding, that of γ-emitter ^{133}Ba increased by only 14% and that of ^{241}Am remained virtually constant (0.04% increase). Although ^{241}Am is an α-emitter and would therefore have a constant internal *DCC* it also has a low-energy γ-decay, which can explain the small change in *DCC* over time. The ultimate reason for the observed difference between elements is the way different types of particles interact with matter (Turner 2005). The β-particles (electrons or positrons) emitted by ^{90}Sr penetrate less far into living matter than the γ-particles (photons) emitted by ^{133}Ba, while the energy of heavy α-particles inside the organism (He nuclei) is fully contained within the tissue due to the very low travel length of α-radiation in living matter (a few tens of microns). If we look at the shoot dosimetry model itself (Fig. 2A–C), it is immediately clear that these differences in *DCC* lead to similar differences in dose rate and dose. For ^{90}Sr, for example (Fig. 2B), we can deduce that if we were to expose seedlings for 4 days starting at 17 days (408 h) of growth, they would accumulate 78% more dose in their shoots than in a 4-day exposure period that starts 96 h after seeding. For shoots exposed to ^{133}Ba (Fig. 2A) this reduces to 8.5% and for ^{241}Am (Fig. 2C) the dose difference between both 4-days' exposure periods is only 0.023%. These surface plots also show that dose does not accumulate in a linear way as would be the case under assumptions of instant equilibrium, but instead follows the dominating bE^2 term in Eq. (10). Similar calculations can be made for dose rate.

Contrary to the shoots, the root dosimetry does not depend on the timing of the exposure, which simplifies the calculations. However, this also means that the ratio between shoot and root dose (and hence dose rate) changes with timing, which might be of importance in understanding the effects of radioactive exposure on the functioning of the plant as a whole. The conclusion arising from these findings is that shoot dosimetry in *A. thaliana* seedlings is very dependent on the timing of the exposure, especially for β and γ-radiation. It is therefore essential to take into account the growth and uptake parameters in effects studies, even more so when comparing effects between life stages.

We next compare the dose and dose rates obtained using the dynamic dose rate modelling approach with the results from a dose calculation method based on end-of experiment geometry and activity concentration, we compared our internal absorbed dose calculations to those of a model that operates under the assumptions of ERICA, namely, (1) instant equilibrium of tissue activity concentration and (2) constant *DCC*.

$$Dose\ static = AC_{end} \times DCC_{end} \times E \tag{15}$$

with AC_{end} obtained from the measured tissue activity concentration at the end of exposure. In the above equation, DCC_{end} is defined as the *DCC* obtained for the geometry at $t=504$. The surface plots in Fig. 3A–C give the ratio of the dose obtained with the dynamic dose estimate model divided by the dose calculated according to Eq. (15) and this for the full exposure duration. The relative differences between the radiation types are evidently still present, but it is clear that for any radionuclide the 'static' approach would overestimate

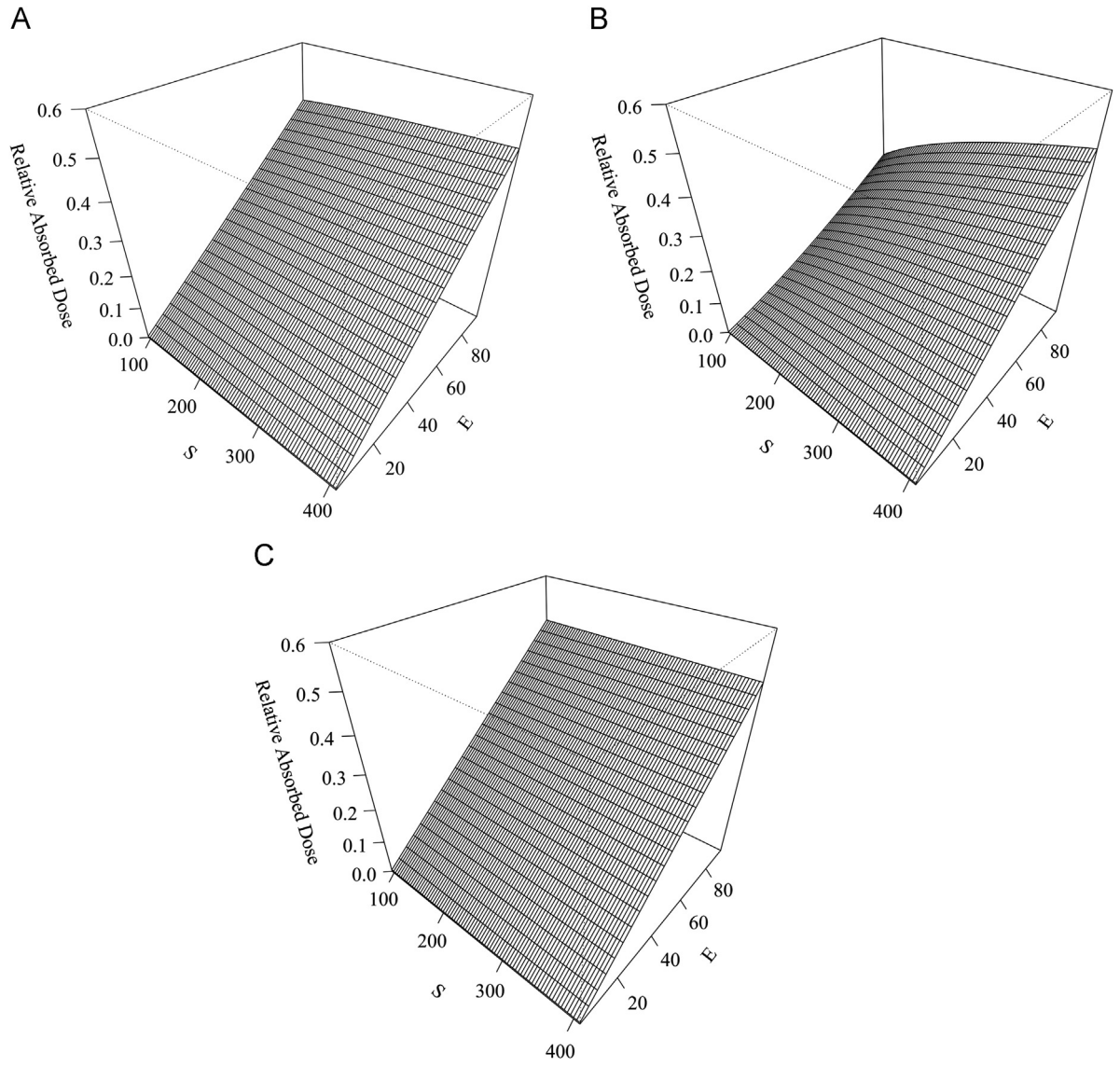

Fig. 3. Comparison of our shoot dose calculations for ^{133}Ba (A), ^{90}Sr (B) and ^{241}Am (C) to calculations under static assumptions. Data from our dynamic model are shown relative to calculations under the classic model for start of exposure S (in hours after sowing) with S=[96 h, 408 h] and exposure length E (in hours) with E=[0 h, 96 h].

the shoot dose at least twofold. The growth effect is again evident if we compare young and old seedlings exposed to ^{90}Sr. The 'static' dose model overestimates doses more (5-fold) at early growth stages (96 h old seedlings exposed for 96 h) that at later growth stages (2-fold, for 408 h old seedlings expose for 96 h). The comparison for ^{241}Am, which has a near constant *DCC*, shows that the observed minimum of twofold overestimation results from the assumption of instant equilibrium, an overestimation which therefore increases in a linear way with decreasing exposure length. This effect of uptake on the difference between both models becomes more manifest when carrying out the comparison for internal root dosimetry, which by definition assumes a constant *DCC* (Eq. (14)). We can calculate the ratio between both models as

$$\frac{\text{Dose dynamic model}}{\text{Dose static model}} = \frac{0.5\, DCC_{root,int}\, \alpha E^2}{AC_{end} \times DCC_{end} \times E} \tag{16}$$

For root dosimetry $DCC_{end} = DCC_{root,int}$ and $AC_{end} = \alpha E_{max}$, which simplifies Eq. (16) to

$$\frac{\text{Dose growth model}}{\text{Dose static model}} = \frac{0.5\, DCC_{root,int}\, \alpha E^2}{\alpha E_{max} DCC_{root,int}\, E} = \frac{0.5\, E}{E_{max}}$$

For $E = E_{max}$, the ratio between the two models equals 0.5, a twofold overestimation by the static model. Eq. (16) only describes the difference in internal root dose caused by inclusion of radionuclide uptake over time.

The above comparison shows that the doses (and dose rates) calculated by the 'dynamic' model are lower than doses calculated by the static dose calculation approach. Dose rate and risk assessment tools such as ERICA or RESRAD are not developed to estimate doses and dose rates during biota development and will give a 'static' dose (rate) (or semi-static—if different geometries and related uptake assessed in a consecutive manner). It would in principle be possible, at least for the shoots, to enter each growth stage's geometry manually in these models and, in this way, obtain *DCC* values which would be identical to those found in our calculations. While this would undoubtedly remove the growth-related bias on the dose estimates, it requires the manual input of each growth stage as a separate organism into the software and furthermore would not remove the overestimation due to the assumption of instant equilibrium. This makes for a very time-consuming approach, as these tools were not designed for such a purpose. The modifications made to the original VBA calculator designed by Vives I Batlle et al. (2004) allow for a fast way to

calculate *DCC* values for a nearly unlimited amount of geometries in batch and therefore constitute a practical improvement for use in situations outside the normal range of application of these tools, where batch calculations are required.

Though our model represents a considerable improvement due to its organ-based approach and the inclusion of seedling growth, several conceptual limits remain that future research will have to address. We have used the radionuclide-specific yet time-constant uptake rate α to describe the accumulation in a tissue when calculating internal dose. Our previous experiments suggested that this rate indeed remains constant throughout the time interval for a given environmental activity concentration. These assumptions have to be addressed more thoroughly if we were to extend the dosimetric model to the entire lifecycle, to other plant models or to other radionuclides. The assumption of linear accumulation not only provides the advantage that just a single measurement of activity concentration is needed, but also allows for dosimetry calculations in field situations where generally only one measurement can be obtained. However, if we were to observe experimentally a different pattern of accumulation than the linear pattern used in this study, the new relationship for *AC(t)* could easily be inserted into the equations. The only remaining mathematical difficulty would be to solve the integration of the dose rate over the exposure.

Our dosimetry model relies on describing a *DCC(t)* relationship, which for the shoots was fitted quite well by a logarithmic function (Fig. 1; Table 2). Even for ^{241}Am, which has a near constant *DCC*, this function allowed to describe the small change in *DCC* caused by the small contribution of γ-decay to the dose. Theoretically, the *DCC* value should converge to a maximum value with increasing rosette diameter, as the fraction of energy absorbed within the geometry approaches unity. The rosette diameter itself is dependent on the typical logistic plant growth curve, and reaches a maximum before flowering (Boyes et al., 2001). Finally, preliminary attempts to expand the model to a longer list of radionuclides (data not shown) have taught us that for many elements the logarithmic relation does not hold true within the whole interval. Hence, while the logarithmic function is a good fit within the studied interval and for the three selected radionuclides, it does not correctly reflect the theoretical physical and biological background.

Our model dispenses with a direct description of growth by calculating the *DCC* for intermediate time points and fitting a curve to the evolution of *DCC* over time. Therefore it still requires the input from a plant culture for which the geometries have been experimentally determined over time, and for which a new set of Monte Carlo calculations has to be carried out if the experimental growth conditions are changed. Ideally, the basis of the model would be a theoretical description of *DCC* as a function of diameter, $DCC=f(D)$, for which the *DCC* calculations have to be performed only once. Any experiment-specific growth function for *A. thaliana* which describes dose as a function of time can then be nested into the diameter-dependent function for *DCC* to produce *DCC(t),* making the resultant function directly dependent on the plant growth parameters, and retaining the theoretical physical background enclosed in the relation of *DCC* to *D*. In addition to *D*, it should therefore also, in principle, be possible to add leaf thickness to the growth parameters. The constant value used in our present model, though representative for the majority of the time period modelled, may not be an accurate assumption at early growth stages.

Though establishing such a theoretical framework goes beyond the scope of this paper, we believe that it would greatly improve the flexibility of our plant dosimetry model. This is true not only with respect to other plant species, but also regarding application to scenarios outside laboratory conditions, where growth can be significantly altered by environmental factors other than radioactive exposure. Several authors have previously stressed the importance of dynamic models in calculating time-integrated doses for release or exposure scenarios (Lepicard et al., 2004; Vives i Batlle et al., 2008). To our knowledge, our study marks the first time that such an approach is proposed for plants with inclusion of growth. Whilst this adumbrates a more general, theoretically underpinned plant dosimetry model, we believe that the concepts put forward in this study can equally be of use in additional organisms where fast growth rate and small geometry might induce rapidly evolving *DCC* values.

We conclude that our model sheds light on how radionuclide doses delivered to *A. thaliana* shoots are highly dependent on the life stage at which the plant is contaminated. Further, the extent of the growth effect depends on the physical properties of the radionuclide. Finally, we have validated our study hypothesis that the absorbed doses (and dose rates) obtained are resulting in more robust dose (rate) predictions, required for establishing more reliable dose–effect relationships and hence finally leading to more realistic assessments in radiological environmental protection and derivation of more robust protection benchmarks.

Acknowledgements

This research was funded by the Research Foundation Flanders (FWO) grant no. 1.1.763.10N in joint funding with SCK●CEN.

References

Andersson, P., Garnier-Laplace, J., Beresford, N.A., Copplestone, D., Howard, B.J., Howe, P., Oughton, D., Whitehouse, P., 2009. Protection of the environment from ionising radiation in a regulatory context (protect): proposed numerical benchmark values. J. Environ. Radioact 100, 1100–1108.

Beresford, N.A., Barnett, C.L., Beaugelin-Seiller, K., Brown, J.E., Cheng, J.-J., Copplestone, D., Gaschak, S., Hingston, J.L., Horyna, J., Hosseini, A., Howard, B.J., Kamboj, S., Kryshev, A., Nedveckaite, T., Olyslaegers, G., Sazykina, T., Smith, J.T., Telleria, D., Vives i Batlle, J., Yankovich, T.L., Heling, R., Wood, M.D., Yu, C., 2009. Findings and recommendations from an international comparison of models and approaches for the estimation of radiological exposure to non-human biota. Radioprotection 44, 565–570.

Berger, M.J., 1968. Energy deposition in water by photons from point isotropic sources. J. Nucl. Med. 9, 15–25.

Berger, M.J., 1971. Distribution of absorbed dose around point sources of electrons and beta particles in water and other media. J. Nucl. Med Suppl. 5, 5–23.

Biermans, G., Horemans, N., Vanhoudt, N., Vandenhove, H., Saenen, E., Ven Hees, M., Wannijn, J., Vives i Batlle, J., Cuypers, A., 2013. An organ-based approach to dose calculation in the assessment of dose-dependent biological effects of ionizing radiation in *Arabidopsis thaliana*. J. Environ. Radioact , http://dx.doi.org/10.1016/j.jenvrad.2013.03.011

Boyes, D.C., Zayed, a.M., Ascenzi, R., McCaskill, a.J., Hoffman, N.E., Davis, K.R., Görlach, J., 2001. Growth stage-based phenotypic analysis of *Arabidopsis*: a model for high throughput functional genomics in plants. Plant Cell 13, 1499–1510.

Brown, J.E., Alfonso, B., Avila, R., Beresford, N.a., Copplestone, D., Pröhl, G., Ulanovsky, A., 2008. The ERICA tool. J. Environ. Radioact 99, 1371–1383.

Copplestone, D., Bielby, S., Jones, S.R., Patton, D., Daniel, C.P., Gize, I., 2001. Impact Assessment of Ionising Radiation on Wildlife. Environment Agency, UK and English Nature (R&D Publication 128)

DOE, 2011. Radiation Protection of the Public and the Environment. DOE Order 458.1. U.S. Department of Energy, Office of Health, Safety and Security.

Davison, A.C., Hinkley, D.V., 1997. Bootstrap Methods and their Application. Cambridge University Press (Cambridge Series in Statistical and Probabilistic Mathematics)

Elzhov, T.V., Mullen, K.V., Bolker, B., 2010. minpack.lm: R Interface to the Levenberg–Marquardt Nonlinear Least-squares Algorithm found in MINPACK. R Package Version 1.1-5. http://CRAN.R-project.org/package=minpack.lm.

Garnier-Laplace, J., Gilbin, R. (Eds.), 2006. ERICA DELIVERABLE 5: Derivation of Predicted-No-Effect-Dose-Rate Values for Ecosystems (and their Sub-organisational Levels) Exposed to Radioactive Substances.

Garnier-Laplace, J., Gilek, M., Sundell-Bergman, S., Larsson, C.M., 2004. Assessing ecological effects of radionuclides: data gaps and extrapolation issues. J. Radiol. Prot. 24, 139–155.

Gulsen, M., Smith, A.E., Tate, D.M., 1995. A genetic algorithm approach to curve fitting. Int. J. Prod. Res. 33, 1911–1923.

Hinton, T.G., Garnier-Laplace, J., Vandenhove, H., Dowdall, M., Adam-Guillermin, C., Alonzo, F., Barnett, C., Beaugelin-Seiller, K., Beresford, N.A., Bradshaw, C., Brown,

J., Eyrolle, F., Fevrier, L., Gariel, J.-C., Gilbin, R., Hertel-Aas, T., Horemans, N., Howard, B.J., Ikäheimonen, T., Mora, J.C., Oughton, D., Real, A., Salbu, B., Simon-Cornu, M., Steiner, M., Sweeck, L., Vives i Batlle, J., 2013. An invitation to contribute to a strategic research agenda in radioecology. J. Environ. Radioact 115 (**73–82.1**).

IAEA, 2010. Handbook of Parameter Values for the Prediction of Radionuclide Transfer in Terrestrial and Freshwater Environments. Technical Report Series 472.

ICRP, 2009. Environmental Protection: The Concept and Use of Reference Animals and Plants. ICRP Publication 108, Ann. ICRP 37 (4-6).

Leister, D., Varotto, C., Pesaresi, P., Niwergall, A., Salamini, F., 1999. Large-scale evaluation of plant growth in *Arabidopsis thaliana* by non-invasive image analysis. Plant Physiol. Biochem 37, 671–678.

Lepicard, S., Heling, R., Maderich, V., 2004. POSEIDON/RODOS models for radiological assessment of marine environment after accidental releases: application to coastal areas of the Baltic, Black and North Seas. J. Environ. Radioact 72, 153–161.

Marquardt, D.W., 1963. An algorithm for least-squares estimation of non-linear parameters. SIAM J. Appl. Math. 11, 431–441.

Psaltaki, M., Brown, J.E., Howard, B.J., 2013. TRS Cs $CR_{wo\text{-}water}$ values for the marine environment: analysis, applications and comparisons. J. Environ. Radioact. 126, 367–375, http://dx.doi.org/10.1016/j.jenvrad.2012.07.001.

R Development Core Team. 2011. R: A Language and Environment for Statistical Computing. R Foundation for Statistical Computing, Vienna, Austria.

Schneider, C.A., Rasband, W.S., Eliceiri, K.W., 2012. NIH Image to ImageJ: 25 years of image analysis. Nat. Methods 9, 671–675.

Turner, J.E., 2005. Interaction of ionizing radiation with matter. Health Phys. 88, 520–544.

Vives I Batlle, J., Jones, S.R., Gómez-Ros, J.M., 2004. A method for calculation of dose per unit concentration values for aquatic biota. J. Radiol. Prot. 24, 13–34.

Vives I Batlle, J., Wilson, R.C., Watts, S.J., Jones, S.R., McDonald, P., Vives-Lynch, S., 2008. Dynamic model for the assessment of radiological exposure to marine biota. J. Environ. Radioact. 99, 1711–1730.

Vives I Batlle, J., 2011. Impact of nuclear accidents on marine biota. Integr. Environ. Assess. Manage 7, 365–367.